Surface formation routes of interstellar molecules : a laboratory study

Sergio, I.

CHAPTER 6

Water formation by surface O_3 hydrogenation[1]

Three solid state formation routes have been proposed in the past to explain the observed abundance of water in space: the hydrogenation reaction channels of atomic oxygen (O + H), molecular oxygen (O_2 + H) and ozone (O_3 + H). New data are presented here for the third scheme with a focus on the reactions O_3 + H, OH + H, and OH + H_2, which were difficult to quantify in previous studies. A comprehensive set of H/D-atom addition experiments is presented for astronomically relevant temperatures. Starting from the hydrogenation/deuteration of solid O_3 ice, we find experimental evidence for H_2O/D_2O (and H_2O_2/D_2O_2) ice formation using Reflection Absorption InfraRed Spectroscopy (RAIRS). The temperature and H/D-atom flux dependence are studied and this provides information on the mobility of ozone within the ice and possible isotope effects in the reaction scheme. The experiments show that the O_3 + H channel takes place through stages that interact with the O and O_2 hydrogenation reaction schemes. It is also found that the reaction OH + H_2 (OH + H), as an intermediate step, plays a prominent (less efficient) role. The main conclusion is that solid O_3 hydrogenation offers a potential reaction channel for the formation of water in space.

[1]Based on: C. Romanzin, S. Ioppolo, H. M. Cuppen, E. F. van Dishoeck, H. Linnartz, 2010, submitted to Journal of Chemical Physics

6.1 Introduction

Water is ubiquitous throughout the Universe and belongs to the more abundant species in the interstellar medium. Since gas phase formation rates are not efficient at low temperatures, the formation of H_2O ice in cold dense quiescent interstellar clouds (~10 K) is expected to take place in the solid state on the surface of dust grains through H-atom addition reactions. Three different hydrogenation channels have been proposed in the past: O + H, O_2 + H and O_3 + H (Tielens & Hagen 1982). Several laboratory studies investigated the formation of solid H_2O through the hydrogenation of atomic oxygen (Hiraoka et al. 1998, Dulieu et al. 2010) and molecular oxygen (Miyauchi et al. 2008, Ioppolo et al. 2008, Matar et al. 2008, Oba et al. 2009, Ioppolo et al. 2010, Cuppen et al. 2010). However, only a single study (Mokrane et al. 2009) investigated the third channel so far, showing that the deuteration of O_3 ice on an amorphous H_2O substrate leads to the formation of D_2O by detecting HDO molecules during desorption of the ice using Quadrupole Mass Spectrometry (QMS). We give here further experimental evidence for H_2O/D_2O ice formation, presenting for the first time a comprehensive set of H/D-atom addition experiments on solid O_3 for astronomically relevant temperatures, using Reflection Absorption InfraRed Spectroscopy (RAIRS).

Solid O_3 can be formed in space through energetic processing (ions, photons, electrons) of O-bearing ices at astronomically relevant temperatures (*e.g.*, Famá et al. 2002, Loeffler et al. 2006, Cooper et al. 2008, Schriver-Mazzuoli et al. 1995, Gerakines et al. 1996, Lacombe et al. 1997, Bennett & Kaiser 2005, Sivaraman et al. 2007). Tielens & Hagen (1982) proposed the formation of O_3 ice through the subsequent oxidation of atomic oxygen on the surface of the interstellar grains at low temperature and in absence of UV irradiation. Ozone ice has been observed on the surface of small bodies in the Solar System, like Ganymede, Rhea and Dione (Noll et al. 1996, 1997, Hendrix et al. 1999), but it has not been observed in the interstellar medium. The non-detection of solid ozone in dense molecular clouds is consistent with an efficient use-up through hydrogenation, in the case that O_3 + H is an efficient process under interstellar conditions.

Figure 6.1 is taken from Chapter 5 and shows how the three hydrogenation channels ($O/O_2/O_3$ + H) can interact. Specifically, the hydrogenation of solid O_3 comprises the following solid-state reactions

$$O_3 + H \rightarrow OH + O_2 \tag{6.1}$$

$$OH + H \rightarrow H_2O, \tag{6.2}$$

and

$$OH + H_2 \rightarrow H_2O + H. \tag{6.3}$$

Cuppen & Herbst (2007) and Cazaux et al. (2010) showed in their astrochemical models that the efficiency of this reaction channel strongly depends on the astronomical environment (*e.g.*, diffuse clouds, dense clouds and photon-dominated regions). The experimental results presented in Chapters 4 and 5 showed that the O + H and the O_3 + H channels are connected *via* the O_2 + H route through common reactive intermediates (see Fig. 6.1).

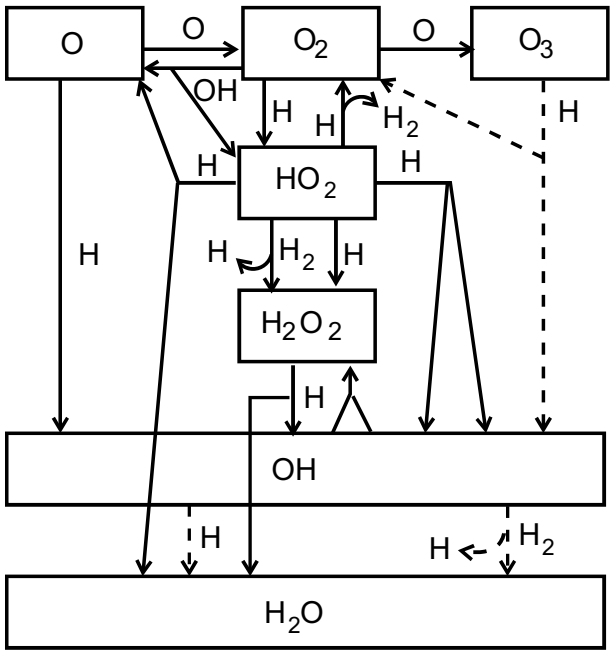

Figure 6.1 A schematic representation of the reaction network as obtained from Chapters 4, 5 and 6. The dashed arrows represent the surface reactions investigated here.

The latter channel involves the reactions

$$HO_2 + H \rightarrow H_2O + O \tag{6.4}$$

and

$$O_2 + OH \rightarrow HO_2 + O, \tag{6.5}$$

which both lead to the formation of O atoms. These can then react with O_2 to form O_3

$$O_2 + O \rightarrow O_3. \tag{6.6}$$

Indeed, O_3 has been found as a reaction product in hydrogenation experiments of pure O_2 ice (Chapters 4 and 5).

In the following sections we investigate the O_3 + H scheme under interstellar analog conditions. We focus in particular on the first reaction step O_3 + H as well as the formation of H_2O from OH through reactions (6.2) and (6.3). For this purpose, most experiments are carried out at elevated temperatures in order to instantaneously desorb the O_2 formed through reaction (6.1).

6.2 Experimental procedure

Experimental details

The experiments are performed using an ultra high vacuum set-up, which has been described in detail elsewhere (Chapters 2 and 4). It consists of an atomic beam line and a main chamber ($\sim 10^{-10}$ mbar), in which ices are grown on a (12−300 K) cryogenically cooled gold-coated copper substrate by depositing gas under an angle of 45°. A fresh O_3 sample is prepared before each experiment in a high-vacuum glass line, following the procedure as described in Berkley et al. (1988). The O_3 sample is prepared in a commercial ozone generator (Fischer-model 502, O_2 99.995% of purity, Praxair) and collected in a liquid nitrogen trap, which is used to purify the sample from O_2 pollution. O_2 deposition originating from the dissociation of O_3 in the main chamber is kept to a minimum by maintaining the substrate temperature at 40 K, well above the O_2 desorption temperature ($T_{\rm des}(O_2)$ ~30 K, Acharyya et al. 2007). The ice is monitored by means of RAIRS, using a Fourier Transform InfraRed spectrometer (FTIR). The FTIR covers the range between 4000 and 700 cm^{-1} (2.5−14 μm) with a spectral resolution of 1 cm^{-1}. A co-addition of 256 scans yields one spectrum. RAIR difference spectra (ΔA) with respect to the deposited O_3 ice spectrum are acquired every few minutes during the hydrogenation experiment. According to Sivaraman et al. (2007), shape and position of the $\nu_3(O_3)$ stretching mode is sensitive to the ozone environment. Therefore, the presence of other molecules should affect this infrared band, but the observed $\nu_3(O_3)$ band in our spectra after deposition is typical for a rather pure O_3 ice (Sivaraman et al. 2007, Chaabouni et al. 2000, Misochko et al. 1999), instead of O_3 molecules mixed with O_2 (Schriver-Mazzuoli et al. 1995).

After deposition the ice is subsequently hydrogenated/deuterated at different temperatures (25, 40 and 50 K). H/D atoms are supplied by a well-characterized thermal cracking source (Tschersich & von Bonin 1998, Tschersich 2000, Tschersich et al. 2008). H_2/D_2 molecules are cracked in a capillary pipe surrounded by a tungsten filament, which is heated to 2200 K. During the H/D-atom exposure, the pressure in the atomic line is kept constant. Hot H/D atoms are cooled to room temperature via collisions by a nose-shaped quartz pipe, placed in the H/D-atom beam path towards the substrate. The geometry of the pipe is designed in such a way that hot species (H/D; H_2/D_2) cannot reach the ice directly (more details in Chapters 2 and 4). The H/D-atom fluxes used in our experiments are set by changing the H_2/D_2 pressure in the capillary pipe while the filament temperature is kept constant. The final flux values (2×10^{13} and 8×10^{13} atoms cm^{-2} s^{-1} for H atoms and 1×10^{13} and 4×10^{13} atoms cm^{-2} s^{-1} for D atoms) are measured at the substrate position in the main chamber using a quadrupole mass spectrometer for the D-atom flux. The method is described in the Appendix A of Chapter 4. The relative error in the D-atom flux determination is within 10%, while the relative H-atom flux determination is within 50%. The absolute error for both is estimated to be within 50%.

Several control experiments have been carried out. Deuteration experiments have been performed to estimate the maximum H_2O contamination, *i.e.*, H_2O contributions other than those induced in the ice upon H-atom impact. This is essential as H_2O is

the prime target of this study. The pollution may originate from H_2O background in the UHV setup and/or from H_2O in the HV gas line. The contamination is found to increase with time and to be less ~1 ML at the end of all experiments. Results presented in § 6.3 are corrected for this contamination. In the deuteration experiments, naturally, this contamination does not play a role. Also, a pure O_3 ice has been exposed to a D_2 beam (at 40 K) to ensure that the D_2 molecules do not chemically react with the O_3 or physically change the surface through sputtering. Finally, an unprocessed O_3 ice grown at 40 K and subsequently heated to 50 K with a rate of 1 K min^{-1}, shows no substantial O_3 loss because of thermal desorption ($T_{des}(O_3)$ ~63 K, Famá et al. 2002) over a three hour period, the length of a typical experiment.

Data analysis

After subtracting the infrared spectra with a piece-wise straight baseline, the column densities (molecules cm^{-2}) of the newly formed species are calculated using the modified Lambert-Beer equation: $N_X = \int A(\nu)d\nu / S_X$, where $A(\nu)$ is the wavelength dependent absorbance. Since literature values of transmission band strengths cannot be used directly in reflection measurements, an apparent absorption band strength, S_X of species X, is determined by individual calibration experiments. This procedure has been described in detail elsewhere (for the H_2O/D_2O and H_2O_2/D_2O_2 band strength determination see Chapters 4 and 5). Briefly, a layer of the selected ice is deposited at a temperature lower than its desorption temperature. The sample is then linearly heated, close to its desorption temperature. Infrared spectra are acquired regularly until the desorption of the ice is complete. Such an isothermal desorption experiment has been performed to determine the apparent absorption band strength of O_3 by recording the transition from zeroth-order to first-order desorption. This is assumed to occur at the onset of the submonolayer regime and appears in the desorption curve as a sudden change in slope. The apparent absorption strength in cm^{-1} ML^{-1} is then calculated by relating the observed integrated area to 1 ML in the modified Lambert-Beer equation. We estimate the uncertainty of the band strength to be within 50%. The noise in the infrared spectra introduces an extra uncertainty in the H_2O/D_2O, H_2O_2/D_2O_2 and O_3 column densities, which is found to be within ±0.5 ML for all the considered species.

The assignment of the spectral features observed in our experiments is listed in Table 6.1. The band modes peaking at 1650/1210 cm^{-1} (ν_2) and 1390/1050 cm^{-1} (ν_2, $2\nu_4$ and ν_6) are chosen to quantify the column densities of the newly formed species upon H/D-atom exposure (solid H_2O/D_2O and H_2O_2/D_2O_2, respectively). The O_3 band peaking at 1050 cm^{-1} (ν_3) is used to quantify the amount of O_3 deposited on the cold substrate, and, subsequently, the O_3 consumed in the surface reactions during H/D-atom addition. The 1050 cm^{-1} D_2O_2 band overlaps with the $\nu_3(O_3)$ band in our infrared spectra. Thus, a multi-Gaussian fit is used to separate the contributions and determine the area of the individual bands.

Table 6.1 Assigned infrared features in the 4000−700 cm^{-1} region.

Mode	Position[a] (cm^{-1})	Species	Position[a] (cm^{-1})	Species	Reference
libration	830	H_2O			1, 2
ν_3	888	H_2O_2	884	D_2O_2	1, 3
ν_2, $2\nu_4$, ν_6	1390(∗)	H_2O_2	1050(∗)	D_2O_2	1, 3
ν_2	1650(∗)	H_2O	1210(∗)	D_2O	1, 2
$2\nu_6$	2840	H_2O_2	2100	D_2O_2	1, 3
ν_1, ν_5	3290	H_2O_2	2465	D_2O_2	1, 3
ν_3	3260	H_2O	2440	D_2O	1, 2
ν_3	1050	O_3			4-6
ν_1	1107	O_3			4-6
$\nu_1 + \nu_3$	2110	O_3			4-6

[a] Asterisks mark the features used to determine the integrated absorbance.
(1) Giguère & Harvey (1959); (2) Hornig et al. (1958); (3) Lannon et al. (1971); (4) Bennett & Kaiser (2005); (5) Chaabouni et al. (2000); (6) Brosset et al. (1993).

6.3 Results and discussion

Figure 6.2 shows the RAIR difference spectra acquired during an hydrogenation (*left panel*) and a deuteration (*right panel*) experiment of solid O_3 at 25 K. Both H_2O/D_2O and H_2O_2/D_2O_2 integrated band intensities clearly grow as the H/D-fluence (H/D-flux × time) increases. Neither species like OH, HO_2, and HO_3, nor the partially deuterated species, like HDO and HDO_2, are detected in our infrared spectra during H/D-atom addition to the O_3 ice. The presence of fully deuterated species gives experimental evidence for surface formation of water ice in the solid phase with O_3 ice as a precursor. The negative peak shown in Fig. 6.2 indeed reflects the O_3 use-up.

6.3.1 Temperature dependence

Figure 6.3 shows the H_2O/D_2O (*square*) and H_2O_2/D_2O_2 (*triangle*) column densities for the three investigated temperatures (25, 40, and 50 K) as a function of the H/D-atom fluence. The solid/open symbols correspond to the low/high H/D-atom flux used in our experiments. The amount of O_3 use-up (*circle*) during H/D-atom addition changes with the substrate temperature from ∼1 ML at 25 K to ∼10 ML at 50 K. This is consistent with the increase of the H/D-atom penetration depth in the O_3 ice at higher temperatures, since the mobility of O_3 molecules in the ice is expected to improve with increasing temperature, even though the penetration depth of H atoms involves only the surface of the ice and not the bulk. A similar temperature dependence has been observed for the penetration depth of H atoms in CO ice (Chapter 2). Another mechanism may also affect the final amount

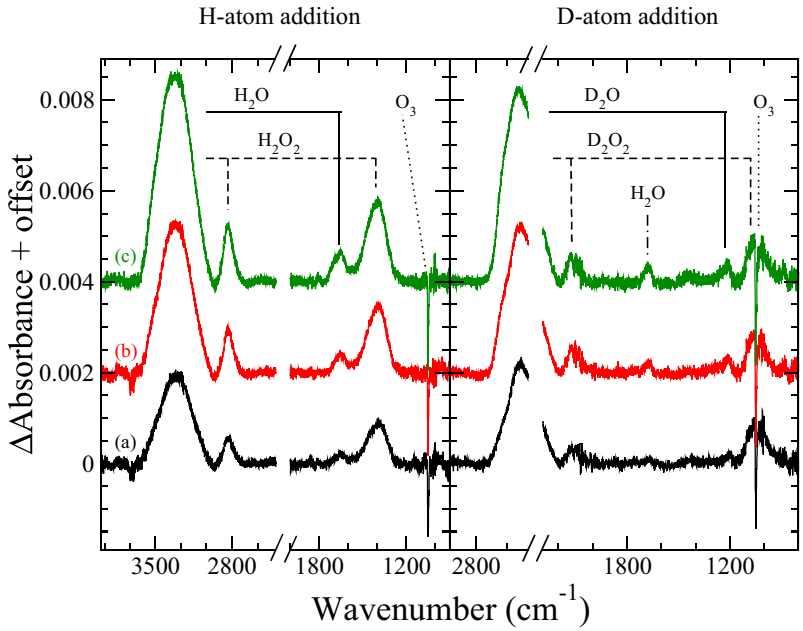

Figure 6.2 Difference infrared spectra of solid O_3 ice, with respect to the spectrum before H/D-atom addition, upon hydrogenation/deuteration at 25 K for three different H/D-atom exposures: (a) 2.4×10^{16}, (b) 7.2×10^{16}, (c) 2.0×10^{17} H/D atoms cm^{-2} s^{-1} (*left/right panel, respectively*). Spectra are offset for clarity. The water pollution is visible in the deuteration experiment (*right panel*).

of O_3 use-up: the erosion of the ice. Each time an H/D atom reacts with an O_3 molecule through reaction (6.1) an O_2 molecule is formed. Whether the O_2 molecule remains on the surface of the ice or desorbs, depends on the temperature of the ice. Below 30 K, the O_2 molecules will be further hydrogenated/deuterated according to the scheme shown in Fig. 6.1 (see also Chapters 4 and 5). At higher temperatures (above 30 K, see Acharyya et al. 2007) the desorption of the O_2 formed through reaction (6.1) will leave the deeper O_3 layers exposed for H/D-atom addition, increasing the final O_3 use-up. The H_2O/D_2O and H_2O_2/D_2O_2 column density ratios are also affected by this desorption behavior. Below 30 K, H_2O/D_2O will be formed through both the hydrogenation/deuteration of O_2 ice and reactions (6.2) and (6.3). A significant amount of H_2O_2/D_2O_2 will be formed through the O_2 channel as well (Chapters 4 and 5). For increasing temperature, the O_2 channel becomes less important and as a consequence the amount of H_2O_2/D_2O_2 decreases, while H_2O/D_2O formation through reactions (6.2) and (6.3) becomes the dominant process.

As a side-effect of the erosion/restructuring of the ice, the H_2O pollution diluted in the O_3 ice, may rearrange in islands. Consequently, the narrow H_2O bands seen after deposition of the O_3 ice in the region of the H_2O bending mode (1650 cm^{-1}) will broaden

Table 6.2 Amounts of O_3 use-up, and formed H_2O/D_2O and H_2O_2/D_2O_2 in ML after an exposure of 1.1×10^{17} H/D atoms cm^{-2} and 4.2×10^{17} H/D atoms cm^{-2} (low and high fluxes, respectively) at the three different substrate temperatures investigated. See §6.2 for the determination of the errors. The O_{budget} corresponds to the mass-balance of O atoms in ML: O_{budget} = -3O_3 + H_2O + 2H_2O_2, or the equivalent for deuteration.

H/D-flux (cm^{-2} s^{-1})	T (K)	O_3	H_2O	H_2O_2 (ML)	O_{budget}	O_3	D_2O	D_2O_2 (ML)	O_{budget}
$2/1 \times 10^{13}$	25	0.8	1.5	4.9	8.9	1.5	1.0	2.7	1.9
	40	2.7	1.8	2.3	-1.7	3.0	1.1	0.6	-6.7
	50	7.4	1.2	0.7	-19.6	8.8	1.8	0.5	-23.6
$8/4 \times 10^{13}$	25	0.8	3.1	4.6	9.9	1.5	1.6	2.2	1.5
	40	2.9	2.9	2.6	-0.6	2.7	1.6	1.4	-3.7
	50	8.1	3.7	1.8	-17.0	8.5	2.2	0.5	-22.3

upon ice restructuring. This effect increases with time and contributes to the total H_2O bulk feature peaking at 1650 cm^{-1}. This effect is shown in the right panel of Fig. 6.2. The contribution of this effect, which is estimated to be ~1 ML at the end of all the deuteration experiments, is taken into account for all the H-atom addition experiments, as mentioned in §6.2.

6.3.2 H/D-atom flux dependence

Figure 6.3 also indicates the influence of the H/D-atom flux on the amount of reaction products. The H_2O/D_2O and H_2O_2/D_2O_2 column densities follow the same trend for high and low H/D-atom flux and for all investigated temperatures within the experimental uncertainties. This observation is in agreement with a scenario in which a reactive system is limited only by the number of H/D atoms that reaches the ice surface. The O_3 column density follows the same behavior for high and low H/D-atom flux at temperatures below 40 K and at 50 K for a maximum H/D-atom fluence of 1×10^{16} H/D atoms cm^{-2}. However, at higher H/D-atom fluence the O_3 column density profile differs for high and low H/D-atom flux at 50 K. This is most likely caused by the transition between two different regimes: in the first regime, reaction (6.1) is limited by the number of H/D atoms, in the second regime, this reaction is limited by the supply of O_3 molecules, since the formed H_2O/D_2O and H_2O_2/D_2O_2 prevent the incoming H/D atoms to reach the O_3 molecules in the lower layers. Further conversion into H_2O/D_2O and H_2O_2/D_2O_2 is then only possible after replenishing of the top layers by fresh O_3. This process is governed by the diffusion of O_3 in the ice, which increases with temperature and is independent of H/D-atom flux. Thus, this effect is stronger at 50 K than at 40 K and indeed the O_3 use-up follows the same trend for low and high H/D-atom fluxes when plotted as a function of exposure time instead of fluence for $>1 \times 10^{16}$ H/D atoms cm^{-2}. The two regimes are schematically depicted in Fig. 6.4.

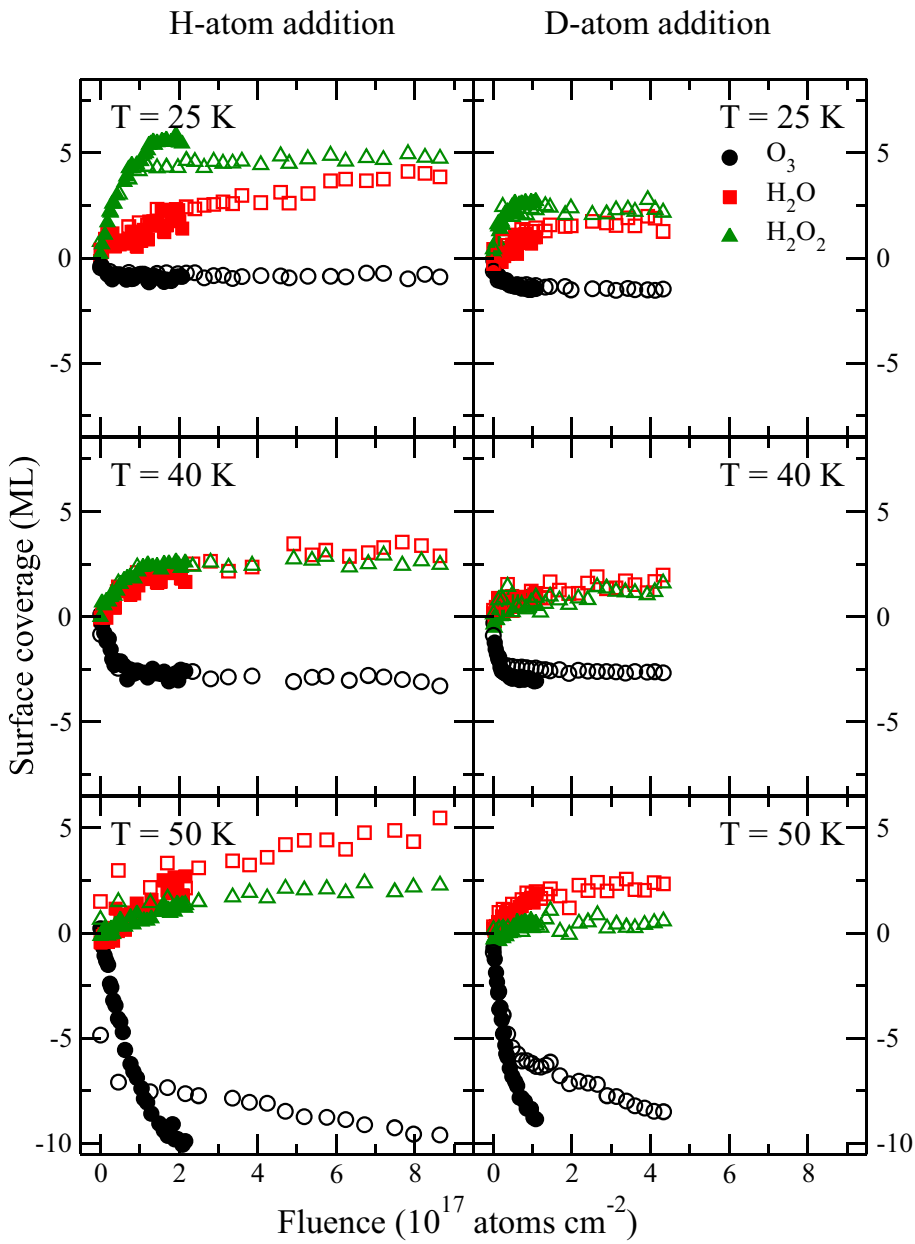

Figure 6.3 Column densities for H_2O/D_2O (*square*), H_2O_2/D_2O_2 (*triangle*) and O_3 (*circle*) for the three temperatures investigated (25, 40, and 50 K) as a function of the H/D-atom fluence. The hydrogenated species are plotted in the left panel, and the deuterated species in the right panel. The solid and open symbols correspond to the lower and higher H/D-atom flux (2×10^{13} and 8×10^{13} atoms cm^{-2} s^{-1} for H atoms, 1×10^{13} and 4×10^{13} atoms cm^{-2} s^{-1} for D atoms), respectively.

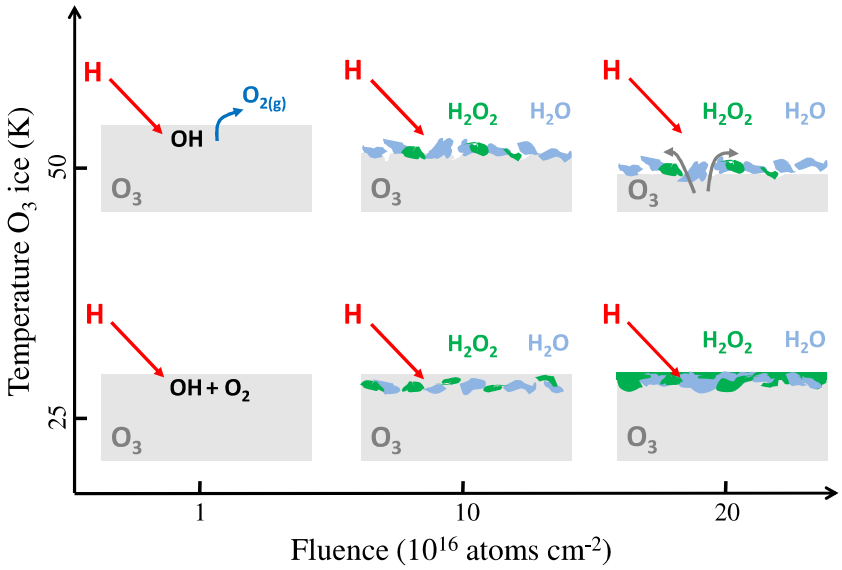

Figure 6.4 Schematic representation of the hydrogenation of O_3 ice as a function of the temperature and H-atom fluence: at temperatures below 40 K (*bottom*) reaction (6.1) is limited by the number of H/D atoms, at higher temperatures (*top*) this reaction is limited by the supply of O_3 molecules. The replenishing of the top layers is induced by diffusion of O_3 in the ice. The erosion of the ice at 50 K is also shown (*top*).

6.3.3 Possible reaction pathways

The investigation of the mass balance between the formed and consumed species in our ice after H/D-atom addition allows identifying the most likely reaction channel responsible for the formation of solid H_2O ice. The mass balance for oxygen atoms can be determined looking at the number of O atoms present in each species (O_{budget} = -3O_3 + H_2O + 2H_2O_2). From the comparison of the results listed in Table 6.2 we summarize three relevant results: (i) the O atoms are found in excess only at 25 K (O_{budget} = 9.9/8.9 ML for higher/lower H-atom flux and 1.5/1.9 ML for both higher/lower D-atom flux); (ii) part of the O use-up is not converted into H_2O/D_2O and H_2O_2/D_2O_2 at 40 and 50 K (negative O_{budget}); and (iii) there appears to be a strong isotope effect in the formation of H_2O/D_2O and H_2O_2/D_2O_2 (more H_2O and H_2O_2 than D_2O and D_2O_2).

Point (i) can be explained by the presence of an extra O_2 poisoning layer deposited on top of the O_3 ice at 25 K. The extra O_2 originates from background deposition, while the substrate was cooled from 40 K to 25 K with a rate of 1 K min^{-1}. This effect is already minimized by lowering the surface temperature only after the main chamber pressure has substantially dropped towards the standard value of 10^{-10} mbar. However, the deposition of a maximum of 5 ML of O_2 on top of the O_3 ice cannot be prevented for the 25 K experiments (5 ML of O_2 correspond to 10 ML of O atoms). The higher value for the

O_{budget} in the 25 K hydrogenation experiment with respect to the deuteration experiment is consistent with a higher penetration depth of H atoms in the O_2 ice compared to D atoms (Chapter 3).

Point (ii) is addressed by the fact that most of the O_2 produced through reaction (6.1) is lost at temperatures higher than the O_2 ice desorption temperature. OH/OD and H_2O/D_2O can desorb upon reaction as well. We will discuss this issue in more detail in the next paragraph, which deals with point (iii).

Roughly the same amount of O_3 is used-up for the hydrogenation and deuteration experiments. This indicates that the observed isotope effect (point (iii)) is not due to a different rate for hydrogenation and deuteration of O_3, but that it is probably caused by a different desorption probability upon reaction. Table 6.2 suggests that D_2O and D_2O_2 are more likely to desorb than H_2O and H_2O_2. Thermal desorption, however, would lead to the reverse and therefore this effect has to come from the reaction energetics. We will first consider H_2O/D_2O, which is formed in two steps. In the first step, reaction (6.1), most of the excess energy will be released in the form of ro-vibrational excitation of OH/OD or in translational energy. Gas phase calculations show that this translational energy is 5.4% higher for deuteration than for hydrogenation (Yu & Varandas 1997), which would lead to a slightly higher desorption probability for D + O_3 than for H + O_3 and may explain at least part of the observed effect. If H_2O/D_2O is then mainly formed from OH/OD through reaction (6.2) (see left side of Fig. 6.5), the large overall difference in desorption probability still cannot be fully explained. It can however be explained if H_2O/D_2O is mainly formed through reaction (6.3). In this case, the kinetic energy is distributed over the products according to the inverse mass which means that D_2O will have nearly twice the kinetic energy of H_2O after reaction (6.3). Since the total excess energy of ~1 eV is close to the desorption energy of H_2O (0.9 eV, Andersson et al. 2006), this difference in kinetic energy will have a substantial effect on the desorption probability. Therefore, in this case more D_2O will desorb from the ice.

The observed isotope effect for H_2O/D_2O can thus be explained by reaction (6.3) instead of reaction (6.2). On first glance one would however expect reaction (6.2) to be more efficient than reaction (6.3), since the first is barrierless, with an excess of 5.3 eV, and the second has a barrier of 0.234 eV (Yang et al. 2001), with an excess of 1 eV. The problem with reaction (6.2) is that one needs to dissipate 5.3 eV of excess energy with just one product. Part of this could be absorbed by the ice surface, but the weak interactions between the product and the ice limits the full dissipation. A reaction where only 1 eV of excess energy is released over two products is therefore more likely, especially since H_2 is abundantly present in our experiment, because the H-atom beam entering the main chamber contains a large fraction of cold H_2.

Furthermore, gas phase experiments indicate that tunneling becomes important for OH + H_2 below 250 K. The reaction rate at 25−50 K will therefore be substantially increased through tunneling. This also leads to an extra isotope effect where OH + H_2 has probably a higher rate than D_2 + OD. In addition, OH/OD is formed "hot" and this energy can also be used to overcome the reaction barrier. Reaction (6.3) may therefore be more relevant than reaction (6.2). These two reactions were previously included in the complete reaction network for O_2 surface hydrogenation investigated in Chapter 5,

although no experimental evidence was found for reaction (6.3). However, the method used there was not very sensitive to the detection of this particular reaction. Therefore, extra dedicated studies specifically on the OH + H_2 reaction are needed to determine the absolute efficiency of this reaction, especially in light of the present study, which indicates that this reaction may be crucial as a final step in all three water formation channels ($O/O_2/O_3$ + H).

Similar arguments can be used for the formation of H_2O_2/D_2O_2 from HO_2/DO_2 by

$$HO_2 + H \rightarrow H_2O_2 \tag{6.7}$$

or

$$HO_2 + H_2 \rightarrow H_2O_2 + H, \tag{6.8}$$

where the latter can again lead to an isotope effect with more D_2O_2 than H_2O_2 desorption and a lower rate of reaction for D_2 + DO_2 through tunneling (see right side of Fig. 6.5). HO_2 + H_2 has a high barrier of 1.1 eV and is endothermic by -0.6 eV. However, in the aforementioned study we have observed this reaction to proceed (Chapter 5). The exothermicity of O_2 + H may help to overcome the barrier and the endothermicity, since the total reaction

$$O_2 + H_2 \rightarrow H_2O_2 \tag{6.9}$$

composed of

$$O_2 + H \rightarrow HO_2, \tag{6.10}$$

and

$$HO_2 + H_2 \rightarrow H_2O_2 + H, \tag{6.11}$$

is exothermic by 1.3 eV.

To summarize, the observed isotope effect between H_2O/H_2O_2 and D_2O/D_2O_2 in the O_3 hydrogenation channel can be explained by a combination of effects. First, OD will get more translational energy than OH in reaction (6.1). Then, if H_2O_2 and H_2O are formed through reactions with H_2, tunneling leads to a higher rate for hydrogenation than deuteration and, secondly, the distribution of excess energy can lead to more D_2O/D_2O_2 than H_2O/H_2O_2 desorption. O_3 is destroyed equally for H and D, which indicates that reaction (6.1) proceeds without substantial tunneling effect.

Finally, all the results discussed here are obtained under laboratory conditions, which in some cases differ order of magnitudes from interstellar conditions (*e.g.*, time scale to reach the same H-atom fluence). Therefore, the use of excess energy to allow further reaction steps, which can proceed under laboratory conditions, might not be favorable under interstellar conditions. For instance, the excess energy of the OH radical formed through reaction (6.1) can be dissipated in the ice before H_2 would reach this OH on interstellar timescales. However, two reaction steps might still apply to the ISM at low temperature (10 K), if an H_2 layer is available on the surface of the ice for further reactions.

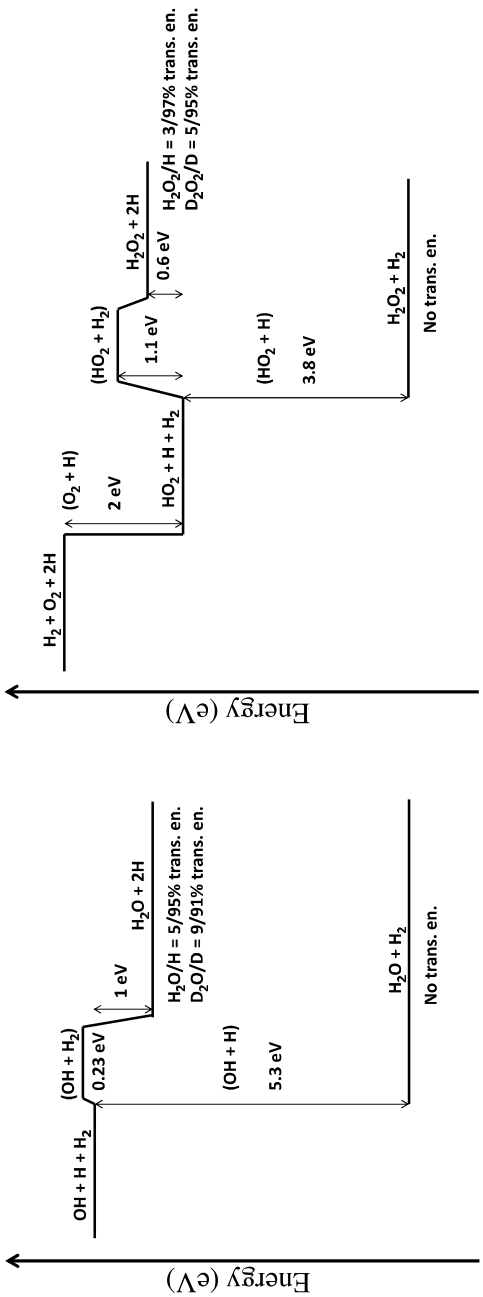

Figure 6.5 Proposed reaction mechanism for the formation of H_2O (*left side*) and H_2O_2 (*right side*) from hydrogenation of O_3 ice. Reactions are shown in brackets.

6.4 Conclusion

The present study shows that the water formation through hydrogenation of solid O_3 ice as proposed by Tielens & Hagen (1982) takes place under interstellar ice analog conditions. Hydrogenation of O_3 ice exhibits a similar temperature dependency as seen for CO ice (Chapter 2): the mobility of O_3 molecules increases with the temperature, while the penetration depth of H atoms into the ice involves only the first monolayers. For temperatures above the O_2 desorption temperature, hydrogenation of O_3 leads to erosion of the ice, since O_2 formed in the reaction O_3 + H desorbs. The remaining OH can further react to H_2O and H_2O_2. The erosion occurs until a layer of H_2O and H_2O_2 layer covers the ice and prevents the incoming H atoms from reaching the underlying O_3 ice. It is found that at high surface temperature (50 K) O_3 is mobile enough to slowly diffuse through the H_2O and H_2O_2 layer and to become available for further hydrogenation on the surface of the ice.

Experimental evidence is found for the connection of the O_3 hydrogenation channel to the O + H and O_2 + H channels, as summarized in Fig. 6.1. As a result it has become possible to draw conclusions on several reactions that are part of the other two hydrogenation channels. The results indicate that the reaction OH + H_2 is most likely more efficient than the reaction OH + H: reaction OH + H_2 could proceed through tunneling, while reaction OH + H needs to dissipate 5.3 eV of excess energy with just one product, which could be difficult. Our experimental results complete the reaction scheme initially proposed in Tielens & Hagen (1982) to explain surface water formation in space. The conclusion that the three channels ($O/O_2/O_3$ + H) are strongly linked, is of importance for astrochemical models focusing on water formation under interstellar conditions.